PCCP

PAPER

View Article Online
View Journal | View Issue

Cite this: *Phys. Chem. Chem. Phys.*, 2018, **20**, 29939

Received 2nd October 2018,
Accepted 14th November 2018

DOI: 10.1039/c8cp06162a

rsc.li/pccp

Two dimensional allotropes of arsenene with a wide range of high and anisotropic carrier mobility

Pooja Jamdagni,*[a] Anil Thakur,[b] Ashok Kumar,[c] P. K. Ahluwalia*[a] and Ravindra Pandey[d]

Considering the rapid development of experimental techniques for fabricating 2D materials in recent years, various monolayers are expected to be experimentally realized in the near future. Motivated by the recent research activities focused on the honeycomb arsenene monolayers, the stability and carrier mobility of non-honeycomb and porous allotropic arsenene are determined using first principles calculations. In addition to five honeycomb structures of arsenene, a total of eight other structures are considered in this study. An extensive analysis comprising energetics, phonon spectra and mechanical properties confirms that these structures are energetically and dynamically stable. All these structures are semiconductors with a broad range of band gaps varying from ~1 eV to ~2.5 eV. Significantly, these monolayer allotropes possess anisotropic carrier mobilities as high as several hundred cm^2 V^{-1} s^{-1} which is comparable with well-known 2D materials such as black phosphorene and monolayer MoS$_2$. Combining such broad band gaps and superior carrier mobilities, these monolayer allotropes can be promising candidates for the superior performance of the next generation nanoscale devices. We further explore these monolayer allotropes for photocatalytic water splitting and find that arsenene monolayers have potential for usage in visible light driven photocatalytic water splitting.

1. Introduction

Due to the variety of structures and fascinating electronic properties, two dimensional (2D) materials offer a promising scenario for next generation electronic devices at the nanoscale. After the successful experimental isolation of black phosphorene,[1,2] its exciting properties[3–6] have resulted in growing interest in the exploration of novel allotropes of group-V monolayers.[7,8] The stability of bulk phosphorus in variety of allotropic forms such as violet-, red-, white- and black-phosphorous has led to theoretical investigations of several allotropes of phosphorene,[9–19] apart from the honeycomb α-P and β-P. All the polymorphs of phosphorene are predicted to be semiconductors with band gaps ranging from 0.4 eV to 2.1 eV.[10–19]

Extensive studies on phosphorene allotropes have encouraged the exploration of the next isoelectronic group-V elemental monolayer *i.e.* arsenene. Similar to α- and β-phosphorene, Kamal *et al.*[20] predicted stable honeycomb structures of As, and Zhang *et al.*[21] investigated the properties of the β-phase of As. In addition, Mardanya *et al.*[22] also confirmed the stability of α-As and β-As with additional stable allotrope γ-As. Ma *et al.*[23] proposed stable tricycle-type monolayer As, and Ersan *et al.*[16] reported a stable square-octagon ring structure monolayer of group-V elements. Apart from the dynamical stability, α- and β-arsenene also exhibit high carrier mobility[24–26] with excellent thermoelectric and device performance.[27–30] The optical response of mono- and bi-layer arsenene (α- and β-phase) shows tunability with mechanical strain.[31] A few other atomically thin allotropes of arsenene were also reported to be dynamically stable.[32,33]

In our previous study,[34] we have identified the role of topological defects in the tunneling characteristics of group-V monolayers including arsenene. It is well known that theoretical predictions often precede experimental synthesis and characterization owing to the difficulties of measurements at the nanoscale. For example, predictions based on first principles calculations[1] have led to realization of a field effect transistor device consisting of a few layers of thick black phosphorene.[2] Likewise, synthesis of blue phosphorene (β-P)[35] has been achieved after its prediction of stability by first principles methods.[9,36] The rapid development in monolayer synthesis

---

[a] *Department of Physics, Himachal Pradesh University, Shimla, H.P., 171005, India. E-mail: j.poojaa1228@gmail.com, pk_ahluwalia7@yahoo.com*

[b] *Department of Physics, Govt. P. G. College, Solan, H.P., 173212, India*

[c] *Department of Physical Sciences, School of Basic and Applied Sciences, Central University of Punjab, Bathinda, 151001, India*

[d] *Department of Physics, Michigan Technological University, Houghton, MI, 49931, USA*

techniques is likely to pave the way for the fabrication of As-based monolayer allotropes in the near future.

In this paper, we consider non-honeycomb (*i.e.* ε-, ξ- and 4-6-10-As) and porous (*i.e.* η-, θ-, hexstar- and K-As) allotropes of arsenene besides the widely studied α-, β-, γ-, δ-, tricycle-type- and square-octagon-As structures. The nomenclature of the arsenene allotropes was taken from that adopted for phosphorene allotropes. Density functional theory calculations were preformed to predict the stability (both energetically and dynamically) and electronic properties of all the monolayer structures of arsenene, including the carrier transport properties, using the phonon-limited scattering model. Finally, as a case study from a practical point of view, we have examined the possibility of application of these monolayers as water splitting photocatalysts.

2. Computational model

Our theoretical analysis and predictions are based on density functional theory (DFT) as implemented in the Vienna ab initio simulation package (VASP).[37] The electron exchange and correlation are treated within the framework of the generalized gradient approximation (GGA) given by the Perdew–Burke–Ernzerhof (PBE) functional.[38] We have used the projector augmented-wave (PAW) method to describe electron–ion interactions.[39] Contributions from the van der Waals (vdW) interactions are also incorporated in calculations by using the DFT-D2 method of Grimme.[40] A plane wave basis set with a kinetic energy cutoff of 400 eV was used. We adopt the Monkhorst–Pack scheme for *k*-point sampling of Brillouin zone integration with a 12 × 12 × 1 mesh. In order to mimic the 2D system, we employ a supercell geometry with a vacuum of about 15 Å along the *z*-direction (which is chosen perpendicular to the plane of arsenene). All the structures were fully relaxed using the standard conjugate gradient method, with residual forces smaller than 0.001 eV Å^{-1} on each atom. The energy convergence value between two consecutive steps was chosen to be 10^{-6} eV. Since the GGA-PBE functional underestimates the band gap, we have also applied a correction to the PBE band structure using the screened hybrid functional HSE06 method.[41,42]

The phonon-limited scattering model including the anisotropic characteristics of effective mass, elastic modulus and deformation potential was applied to calculate carrier mobilities of arsenene allotropes:[24,30,43,44]

$$\mu_{2\mathrm{D}} = \frac{e\hbar^3 C^{2\mathrm{D}}}{k_{\mathrm{B}} T m^* m_{\mathrm{a}}{}^* E_{\mathrm{d}}^{\mathrm{i}2}} \tag{1}$$

where k_{B} is the Boltzmann constant, $T = 300$ K is the temperature, and m^* is the effective mass in the transport direction (either $m_x{}^*$ or $m_y{}^*$ along the x and y direction, respectively) which is given as $m^* = \frac{\hbar^2}{\frac{\partial^2 E_0(k)}{\partial k^2}}$, where E_0 is the conduction/valance band energy along the transport direction and $m_{\mathrm{a}}{}^*$ is the average effective mass determined by $m_{\mathrm{a}}{}^* = \sqrt{m_x{}^* m_y{}^*}$. E_{d} represents the deformation potential of holes/electrons along the transport direction determined by $E_{\mathrm{d}}^{\mathrm{i}} = \frac{\Delta E_{\mathrm{i}}}{\Delta l / l_0}$ where ΔE_{i} is the energy change of the *i*th band under compression and dilation of the cell. $C^{2\mathrm{D}}$ is the in-plane elastic modulus which can be derived from:

$$\frac{E - E_0}{S_0} = \frac{C^{2\mathrm{D}}}{2}\left(\frac{\Delta l}{l_0}\right)^2 \tag{2}$$

where $E - E_0$ represents the total energy change, S_0 is the area of the *xy*-plane and $\frac{\Delta l}{l_0}$ represents the deformation in the *x* or *y* direction.

3. Results and discussion

3.1 Structures

In Fig. 1, the top and side views of monolayer allotropes of arsenene together with the Wigner–Seitz cell are shown. We consider three types of monolayer geometric structures, namely: (i) honeycomb, (ii) non-honeycomb and (iii) porous. The honeycomb structures are α-, β-, γ-, δ- and tricycle-type (T)-As, which contain six membered rings and are designated as (6-6)-As. T-As is constructed by in-plane connections of the segments of α-As and β-As. The honeycomb structures of arsenene exhibit armchair and zigzag edges. Non-honeycomb structures are square-octagon (O)-As, ε-P and ξ-P which contain square and octagon units of arsenic atoms and are denoted by (4-8)-As. For ε-As and ξ-As, each unit cell has two As_4 square units, and side views of both resemble the puckered armchair and zigzag structures of α-As and β-As, respectively. Similarly, (4-6-10)-As consists of four, six and ten member rings in non-honeycomb arrangements of atoms. Four porous allotropes namely η-As, θ-As, hex-star (HS)-As and K-As of arsenene are also shown in Fig. 1. The As atoms in HS-As form a hexagonal lattice with a Magen-David-like top view, whereas η-As and θ-As consist of units of As_5 pentagons that are connected by interunit As–As bonds.

The structural and lattice parameters are listed in Table 1. Most of our calculated values are in very good agreement with the available values in the literature, *e.g.*, for α-As, our calculated lattice parameters (a = 3.67 Å, and b = 4.77 Å), and thickness (h = 2.40 Å) values agree well with the other reported values of lattice parameters (a = 3.68 Å, and b = 4.77 Å) and thickness (h = 2.39 Å).[20]

Notably, the shape diversities [Fig. 1] of hexagonal rings in (6-6)-As and octagon rings in (4-8)-As originate from bond angle variation while the bond lengths are found to be nearly the same [Table 1]. The bond angle variation in (6-6)-As is as large as 20 degrees which is more pronounced (~30 degrees) in (4-8)-As structures. The bond length variations in both types of structures are calculated to be < 0.1 Å.

It is important to note that lattice constants 'b' in α-As and 'a' in δ- and T-As show a difference ≥ 0.05 Å in the calculated values using GGA + PBE and GGA + PBE + vdW levels of theory. The thickness, h, in T-As is calculated to be 4.33 Å and 4.41 Å

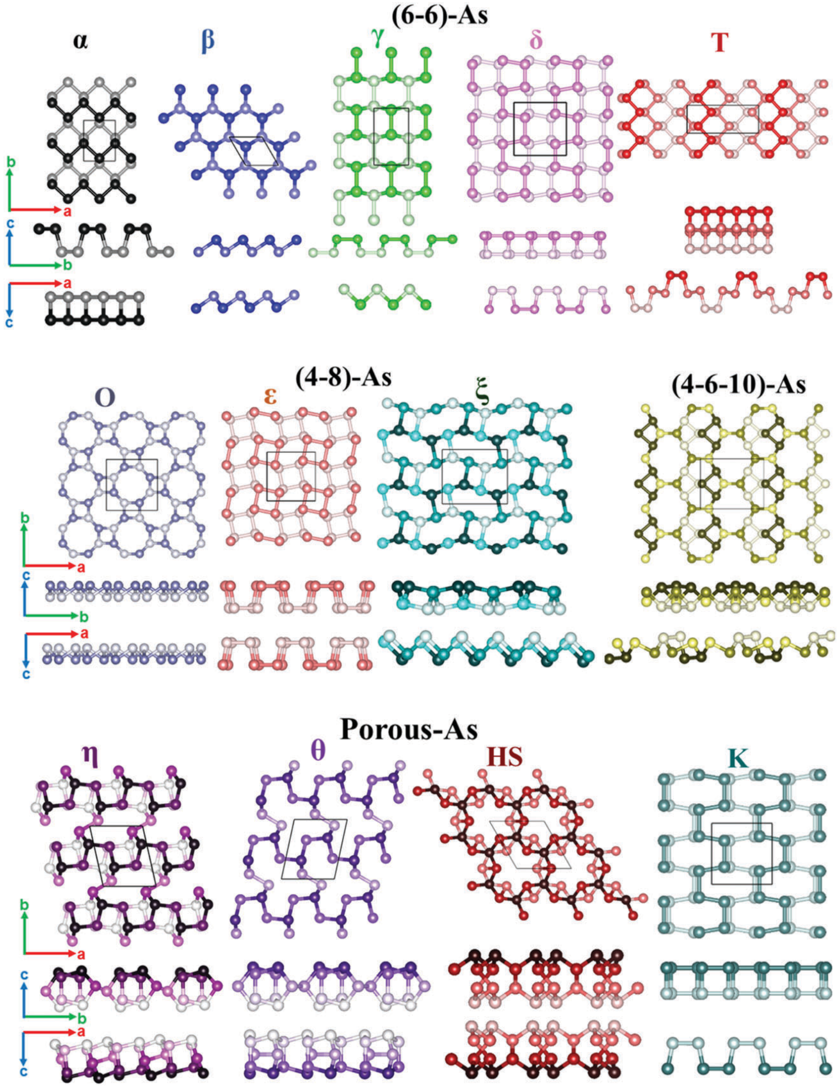

Fig. 1 Top and side views of As-monolayer allotropes with five typical honeycomb 6-member ring structures (α, β, γ, δ, and T); three non-honeycomb (4-8)-member ring structures (O, ε, and ξ); one (4-6-10)-member ring structure and four porous structures (η, θ, HS, and K). Atoms at the top and bottom of nonplanar layers are distinguished by color and shading of atoms (darkest color for the topmost atoms and lightest color for bottommost atoms). The two dimensional unit cell is also shown in the top view of each structure.

using GGA + PBE and GG + PBE + vdW methods, respectively. The results therefore suggest that the vdW correction is important to describe these layered structures with higher thickness. Throughout the study, we have used the PBE functional with vdW correction and the overall results of the study remain nearly the same.

3.2 Stability

(a) Energetics. In order to study the energetics of arsenene monolayers, we calculate their cohesive energy which is given in Table 1. The cohesive energy (E_c) is obtained as the difference between the total energy per atom of arsenene allotropes and the energy of the free As atom. Our calculated value of the cohesive energy (3.19 eV per atom) for α-As is consistent with the previously reported value of 3.13 eV per atom.[22] Despite noticeable structural diversity in (6-6)-As and (4-8)-As allotropes, the cohesive energies are found to lie within a narrow range of 0.07 eV per atom. Among the various variants of arsenene, tricycle-type (T)-As possesses the highest calculated value of cohesive energy (3.20 eV per atom); consequently it is the most stable allotrope followed by α-As, β-As, θ-As, η-As and δ-As. Note that the difference between the cohesive energies of α-, β- and T-As is very small (0.01–0.02 eV) [Table 1]. This is unlike phosphorous allotropes among which the α-phase is found to be the most stable.[9,36] Next, we have calculated the formation energy relative to α-As using the formula:

$$\mathrm{RFE} = \frac{E_{\mathrm{A}} - NE_{\alpha}}{N} \qquad (3)$$

Here E_{A} is the total energy of a given monolayer allotrope, E_{α} is the energy per atom of the α-As monolayer and N is the number of atoms per unit cell of given monolayer allotropes.

Table 1 Calculated values of equilibrium lattice parameters (a, b), thickness (h), bond lengths (d), bond angles (Θ), and cohesive energy (E_c) of arsenene allotropes using the GGA-PBE functional including the van der Waals (vdW) interaction term. N is the number of atoms in a unit cell. The cohesive energy is calculated as: $E_c = |E_T - E_a|$, where E_T and E_a are the total energy per atom of arsenene allotropes and the total energy of an isolated As atom. Other reported GGA-PBE values available in literature are also given

Phase		Space group	N	Structural parameters					E_c (eV per atom)
				a (Å)	b (Å)	h (Å)	d_i (Å)	Θ_i (deg)	
(6-6)-As	α	*Pmna*	4	3.67, 3.68[e] 3.68,[a] 3.68[b]	4.71, 4.77,[e] 4.77,[a] 4.82[b]	2.39, 2.40[e] 2.39[b]	2.48, 2.50 2.49,[a] 2.50,[a] 2.50[b]	94.6, 100.4, 94.6,[a] 100.8,[a] 94.5,[b] 100.2[b]	3.19 3.13[b]
	β	$P\bar{3}m1$	2	$a = b = 3.58$, 3.60,[e] 3.61,[a] 3.61[b]		1.40, 1.38,[e] 1.39[b]	2.51, 2.50,[a] 2.50[b]	91.9, 92.2,[a] 91.7[b]	3.18, 3.15[b]
	γ	*Pmmn*	4	3.57, 3.59[e] 3.58[b]	5.88, 5.90[e] 5.92[b]	1.69, 1.68[e] 1.68[b]	2.49, 2.56 2.50,[b] 2.57[b]	91.9, 98.8 91.7,[b] 98.7[b]	3.13, 3.07[b]
	δ	*Pbcm*	8	5.85, 5.90[e] 5.91[b]	5.90, 5.94[e] 5.93[b]	2.40, 2.38[e] 2.40[b]	2.48, 2.52 2.50[b]	98.6, 100.0 99.1,[b] 99.8[b]	3.15, 3.06[b]
	T	*Pbcm*	8	9.36, 9.57[e] 9.58[c]	3.65, 3.64,[e] 3.65[c]	4.41, 4.33,[e] 4.34[c]	2.49, 2.50 2.51, 2.50[c] 2.51[c]	90.6, 93.5 100.4, 90.5,[c] 93.3,[c] 101.41[c]	3.20
(4-8)-As	O	*P*4/*nbm*	8	$a = b = 7.06$, 7.06[d]		1.41, 1.42[d]	2.48, 2.52, 2.48,[d] 2.52[d]	71.7, 99.3 71.8,[d] 99.4[d]	3.04, 2.98[d]
	ε	$P42_12$	8	$a = b = 5.84$		2.39	2.46, 2.56	90.0, 97.4, 101.5	3.10
	ξ	$P\bar{1}$	8	7.05	5.86	1.69	2.49, 2.56	91.8, 98.9	3.11
(4-6-10)-As		*Pmg*	10	8.45	6.67	2.45	2.49–2.52	81.6–100.9	3.09
Porous-As	η	$P\bar{1}$	10	5.89	6.90	3.97	2.45–2.50	99.3–109.1	3.16
	θ	*Pm*	10	5.95	6.86	3.83	2.46–2.52	83.8–110.3	3.17
	HS	$P\bar{3}1m$	10	$a = b = 6.71$		4.45	2.50, 2.51	48.0–101.6	3.13
	K	$I2_13$	8	5.87	5.95	2.44	2.49, 2.50, 2.55	90.0, 99.8, 101.0	3.08

[a] Ref. 20. [b] Ref. 22. [c] Ref. 23. [d] Ref. 16. [e] Our GGA-PBE calculated values.

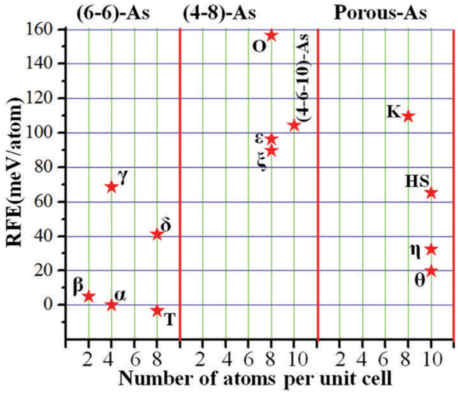

Fig. 2 Relative formation energy (RFE) with respect to α-As, for various monolayer allotropes of As.

All the monolayer allotropes except O-As, (4-6-10)-As and K-As have RFE less than 100 meV [Fig. 2], indicating their ease of formation and energetic stability. The T-As honeycomb monolayer structure has a formation energy of −3.41 meV per atom indicating its stability is higher than α-As. Note that T-As is the in-plane heterostructure allotrope consisting of α and β allotropes of As. It is to be noted that the difference in the RFE of β-As, T-As and θ-As is less than 25 meV per atom [Fig. 2], which is comparable to the thermal energy at room temperature. Note that ξ-As, ε-As, O-As, (4-6-10)-As and K-As possess high RFE (>80 meV) which is attributed to the increased tension in their structures due to 4-membered rings. All other structures possess either five or six membered rings which makes them energetically more favorable. Looking at the existence of so many structures within a very narrow range of RFE, it appears that phase coexistence may indeed be reality in the case of 2D allotropes of arsenene. Note that the bulk form of arsenic *i.e.* grey arsenic exists[45] and β-As monolayers can possibly be exfoliated from bulk As.

(b) Phonon spectra. Next, we computed the phonon dispersion spectra for arsenene allotropes and the results of phonon dispersion along the high symmetry points in the Brillouin zone are presented in Fig. 3. From the phonon spectrum, it is possible to investigate the dynamical stability of a given monolayer. The phonon frequencies are found to be positive for α-, β-, γ-, δ-, T- and ε-As, indicating their dynamical stability. Note that α-, β-, γ- and T-As are also found to be dynamically stable in the previously reported first principles calculations.[20,22,23] In cases of O-, 4-6-10-, ξ-, η- and θ-As, all modes contain positive frequencies except out-of-plane acoustical modes near S and Y high symmetry points [Fig. 3] due to the softening of phonons. Note that a similar prediction was made for β-As[20] and germanene.[46] On the other hand, HS- and K-As possess out-of-plane acoustical modes with imaginary frequency in a large region of the Brillouin zone [Fig. 3], which indicates that these monolayers can only be stabilized on a suitable substrate which can damp the out-of-plane vibrations.

(c) Mechanical properties. The in-plane stiffness of a material is an important parameter to describe its mechanical stability. In order to describe the mechanical properties of given monolayers, we calculate the elastic modulus by fitting the strain energy density curve with in-plane strain [Fig. 4]. The strain energy ($E - E_0$) is obtained by applying a strain (±1.5%) in small steps of 0.05. Different strain energy density curves for

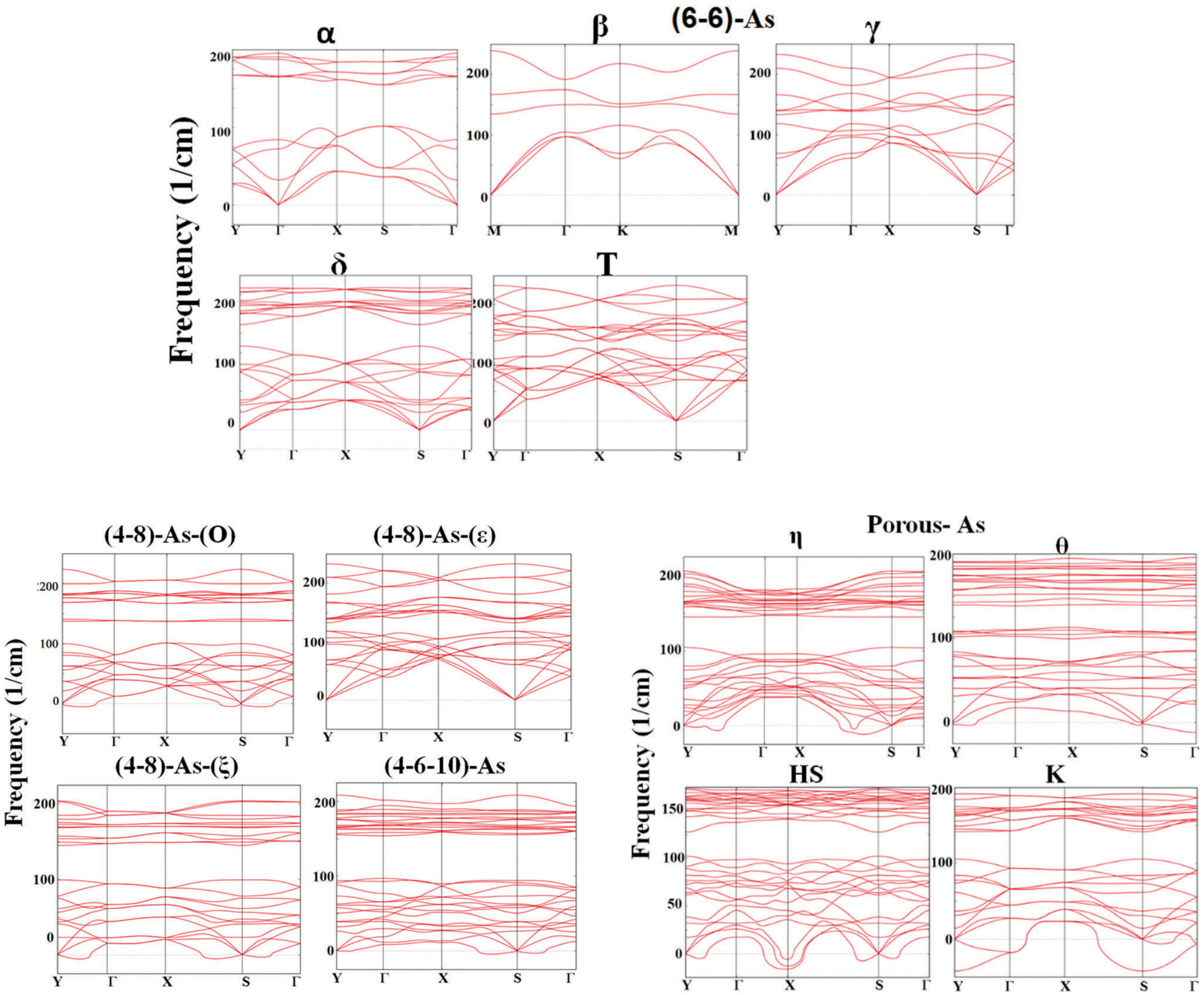

Fig. 3 Phonon dispersion spectra for various monolayer allotropes of As.

strains along the *x*- and *y*-direction are obtained due to the structural anisotropy of arsenene allotropes. For example, C_x^{2D} and C_y^{2D} for α-As are calculated to be 63.8 J m^{-2} and 13.0 J m^{-2}, respectively, which are in very good agreement with the previously reported values of 65.2 J m^{-2} and 16.9 J m^{-2}.[30] β-As possesses isotropic structure with $a = b$; our calculated value of the elastic modulus is 55.5 J m^{-2}, which is in good agreement with the reported value of 51.4 J m^{-2}.[16] The values of the elastic modulus are listed in Table 2. An anisotropic elastic modulus is also evident from the curvature of the strain-energy density *versus* strain curve [Fig. 4], *e.g.*, large curvature of the strain along the *x*-direction in η-As leads to a higher value of the elastic modulus (82.7 J m^{-2}) as compared to small curvature of the strain along the *y*-direction which gives rise to a smaller value of the elastic modulus (40.8 J m^{-2}). The calculated values of the elastic modulus are much smaller than those of some typical 2D materials such as graphene (330 J m^{-2}),[7] h-BN (240 J m^{-2})[47] and MoS$_2$ (180 J m^{-2}),[48] suggesting relatively superior flexibility of arsenene monolayers.

3.3 Electronic band structures

Allotropes of monolayer arsenic are predicted to be semiconductors with a broad range of band gaps which are important for broadband photo-response. γ-As, T-As, O-As and ε-As are direct gap semiconductors while the other monolayers are indirect gap semiconductors [Fig. 5]. Our calculated values of band gaps are in very good agreement with the available values in the literature, *e.g.*, indirect band gaps of α-As (0.72 eV) and β-As (1.58 eV) are in very good agreement with the previously reported values of 0.77 eV and 1.57 eV, respectively;[16] direct band gaps calculated for γ-As (0.79 eV) and O–As (1.81 eV) are consistent with the other reported values 0.86 eV[22] and 1.79 eV,[16] respectively. The calculated values vary from 0.37 eV in K-As to 1.81 eV in O-As. Additionally, the HSE06 hybrid functional calculations predict significantly larger values of band gaps [Table 2] ranging from ∼1 to ∼2.5 eV without changing the nature of the band gaps.

In order to understand the contribution of different orbitals to the electronic states near the Fermi level, we calculate the

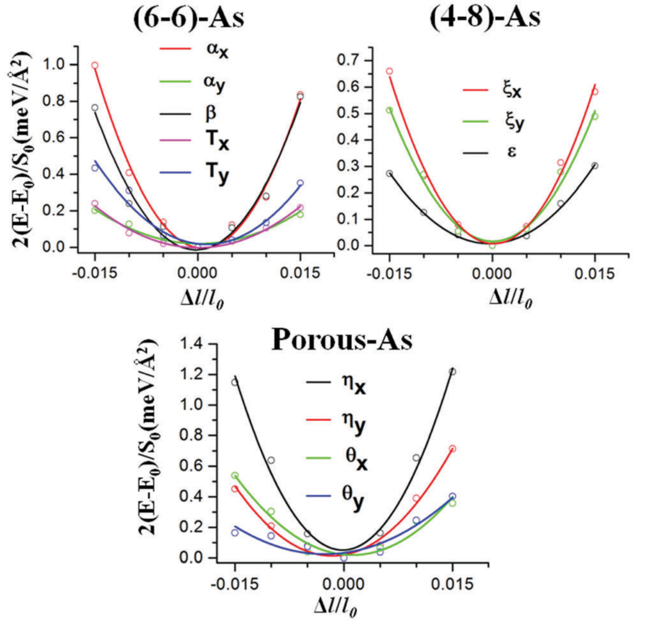

Fig. 4 The 2D elastic modulus obtained from fitting the strain energy density curve $\frac{2(E-E_0)}{S_0}$ *versus* $\Delta l/l$ for low energy allotropes of monolayer As. Uniaxial strain is applied along the x and/or y direction.

Table 2 Calculated values of the elastic modulus (C^{2D}) along the x and y-direction. The band gap (E_g) and workfunction (φ) using the HSE functional for monolayer allotropes of As. Previously reported values are also listed

Structure		C^{2D} (J m^{-2}) x	y	$E_{g\text{-(HSE)}}$ (eV)	$\Phi_{\text{(HSE)}}$ (eV)
(6-6)-As	α	63.8, 65.2[a]	13.0, 16.9[a]	1.38	4.77
	β	55.5, 51.4[b]		2.21	5.55
	γ	49.7	27.6	1.42	5.18
	δ	7.7	6.4	1.09	4.74
	T	16.2	27.5	1.14	4.65
(4-8)-As	O	11.4, 20.9[b]		2.48, 2.47[b]	5.75
	ε	35.4		1.36	5.11
	ξ	43.8	20.1	1.43	5.30
(4-6-10)-As		6.0	6.8	1.63	5.32
Porous-As	η	82.7	40.8	1.64	5.09
	θ	31.9	19.0	1.77	5.17
	HS	3.0		1.74	5.22
	K	2.5	1.4	1.07	4.67

[a] Ref. 30. [b] Ref. 16.

orbital projected density of states (PDOS), which reveals that the states near the valance and conduction-band edges are primarily contributed by p orbitals [Fig. 6]. The fact that the p orbitals are dominant is a common feature of monolayer honeycomb systems such as silicene, germanene and phosphorene, where sp^2-like bonds form non-planar honeycomb structure. A notable contribution from p_z orbitals with out-of-plane electron density perpendicular to the monolayer can be seen in PDOS plots. This is further endorsed by the special distribution of VBM and CBM charge density and can be characterized by the localization of charge on the atomic sites [Fig. 6]. In the case of multilayer structures, these states are going to participate in interlayer hopping with adjacent layers, resulting in a band dispersion perpendicular to the plane. Therefore, multilayer structures of these allotropes are expected to have smaller band gaps than their monolayer structures. A similar effect is observed in phosphorous[36] and transition metal dichalcogenide monolayers,[49] where the band gap is found to be inversely proportional to the number of layers.

A comparison between arsenene allotropes and their predecessor phosphorene allotropes reveals some common features in the electronic band structures due to the similarity in their crystal structures and electronic configurations. For example, energy dispersions of the valance and conduction bands are comparable for similar allotropes belonging to arsenene and phosphorene.[9,11,12,16,17] As a result, β-, ξ-, η-, θ- and HS-As allotropes of arsenene and phosphorene are qualitatively similar being indirect band gap semiconductors. Although the valance and conduction band energies are very close to the respective maximum and minimum at multiple points in Brillouin zones for both arsenene and phosphorere, the valance band maximum (VBM) and conduction band minimum (CBM) are located at different points for equivalent arsenene and phosphorene allotropes, *e.g.*, the location of the VBM in β-As is at Γ whereas for β-P it is in the Γ–K direction; the location of the CBM in ξ-As and ξ-P is at Y and X, respectively. This difference is attributed to the greater delocalization of the valance band edge charge density at the Γ point for β-As and the conduction band edge charge density at the Y point for ξ-As, that leads to the shift in the band energy towards the Fermi level. The greater delocalization at these band edges is due to the hybridization between the in-plane and out-of-plane p orbitals that spatially extend the charge distribution away from the atomic sites [Fig. 6]. Both ε-As and ε-P are direct gap semiconductors with direct transitions at the Γ point. Unlike phosphorene, α- and δ-As monolayers are indirect gap semiconductors, whereas γ-, T- and O-As are direct gap semiconductors. This difference in the nature of the band gap of the two systems may also be attributed to the weaker electronegativity of the As atom as compared to the P atom, that leads to greater delocalization of charge density in As systems and hence a decrease in the VBM/CBM energy towards the Fermi level. It is important to note that the difference between direct and indirect band gaps in γ-, δ-, O-, ε- and (4-6-10)-As is very small ($<$0.03 eV), and a small value of in-plane mechanical strain can induce the direct ↔ indirect gap transition[50] in these monolayers.

3.4 Carrier mobilities

The carrier mobility is a property that is directly related to the electronic conductivity of 2D materials. In the framework of the longitudinal-acoustic phonon dominated scattering mechanism, the carrier mobilities (μ_{2D}) can be calculated using values of the elastic modulus, effective masses and deformation potentials [eqn (1)]. μ_{2D} is directly proportional to the elastic modulus, that is found to be highly anisotropic [Table 2] for all the monolayer allotropes except β-As, O-As, ε-As and HS-As. Essentially,

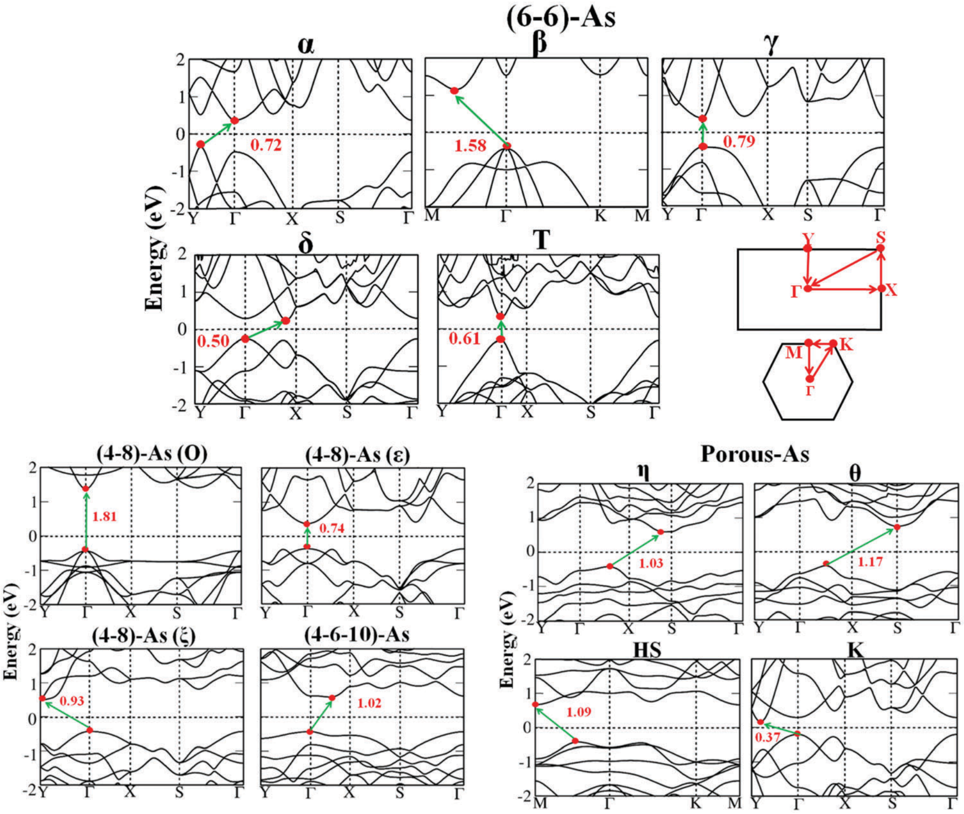

Fig. 5 Electronic band structure of various monolayer allotropes of As calculated using the GGA-PBE method. The Fermi level is set to zero. The Brillouin zones with high symmetry directions are also shown. β-As and HS-As possess hexagonal Brillouin zones while the rest of the monolayers have rectangular Brillouin zones.

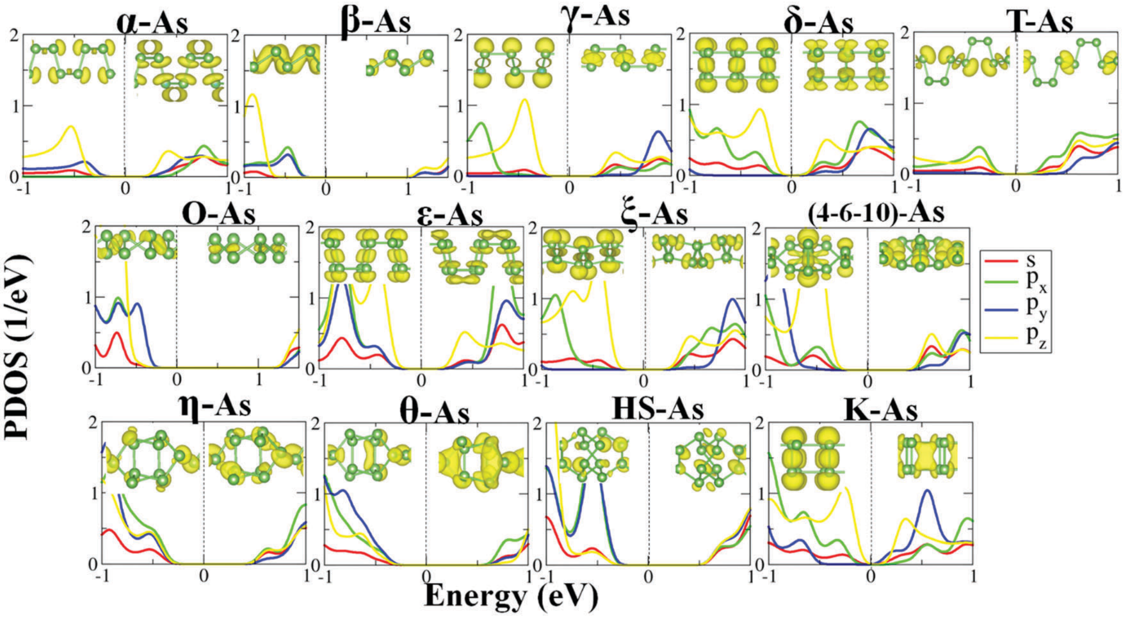

Fig. 6 The orbital projected density of states (PDOS) for the various allotropes of arsenene calculated using the GGA-PBE functional. The p orbitals are dominant for all structures. The vertical dotted line in each plot denotes the Fermi energy which is set at 0 eV. The VBM and CBM charge densities distributions (side views) are represented at the isosurface of 3×10^{-4} e Å^{-3} and superposed with a ball-and-stick model of the structure. Charge density profiles for the valance and conduction band edge are located below and above the Fermi level, respectively, in PDOS plots.

the structural anisotropy in arsenene allotropes leads to anisotropic carrier transport, thereby suggesting that a highly flexible monolayer can give rise to lower carrier mobility and *vice versa*. And, the anisotropic elastic modulus can be attributed to the bonding structure of these allotropes. Under uniaxial strain along the *y*-direction, the bond angles can be modified compared to those along the *x*-direction that may lead to a different superposition of atomic orbitals in both *x*- and *y*-directions. Furthermore, the carrier mobility not only depends on the mechanics of the monolayer, but has also a strong dependence on the carrier effective masses. Note that μ_{2D} is inversely proportional to the product of the carrier effective masses along the transport direction and the average effective masses. The carrier effective masses along the *x*- and *y*-direction are calculated by fitting the *E vs. k* diagram along the Γ–X and Γ–Y direction, respectively, and are listed in Table 3. Our calculated values of electron and hole effective masses for α-As ($m_{e\text{-}x}^* = 1.29$, $m_{e\text{-}y}^* = 0.39$, $m_{h\text{-}x}^* = 1.57$ and $m_{h\text{-}y}^* = 0.21$) are in close agreement with the previously reported values ($m_{e\text{-}x}^* = 1.17$, $m_{e\text{-}y}^* = 0.24$, $m_{h\text{-}x}^* = 1.64$ and $m_{h\text{-}y}^* = 0.13$).[30] For β-As, m_e^* and m_h^* are calculated to be 0.13 and 0.53, respectively, which is in excellent agreement with the other reported values 0.128 and 0.501.[27] Due to the highly isotropic structural arrangement of As atoms in the honeycomb lattice of β-As, it has nearly the same carrier effective masses along *x*- and *y*-directions which is also evident from the symmetric *E vs. k* dispersion around Γ in the electronic band structure of β-As [Fig. 5]. The carrier effective masses are calculated to be highly anisotropic for the monolayer allotropes having structural anisotropy. For example the effective masses of electrons (holes) for ξ-As and η-As along the Γ–X/Γ–Y direction are calculated to be 0.55/4.85 (1.73/1.52) and 1.40/3.47 (3.52/1.68). The carrier effective masses at the VBM/CBM are listed in Table 3.

Another key factor which also determines the carrier mobility is the deformation potential ($\mu_{2D} \propto 1/E_d^2$) and it is calculated by the linear fitting of the VBM/CBM *vs.* strain surface. The magnitude of E_d describes the change in energy of the electronic band with the elastic deformation and, therefore, describes the degree to which the charge carriers interact with phonons. A lower value of E_d indicates weaker electron–phonon coupling in the conduction (valence) band, thereby contributing to an increase in the mobility of electrons (holes).[43,44] The deformation potential shows significant dependence on both transport direction and types of carriers. For example for α-As, the value of E_d for holes along the *y*-direction is 3.5 times more than the value in the *x*-direction whereas the value of E_d for electrons along the *y*-direction is 2.5 times less than the value in the *x*-direction. The values of E_d for electrons and holes along *x*- and *y*-directions are listed in Table 3.

Incorporating the anisotropic characteristics of the elastic modulus, effective masses and deformation potentials, we have calculated the carrier mobilities at $T = 300$ K. Our calculated values of carrier mobilities show directional anisotropy and are found to be, in general, moderately high [Fig. 7]. For example hole (electron) mobility of α-As along the *x*-direction is 7.5 (4) times higher than the mobility along the *y*-direction. The hole (electron) mobilities of ξ-As vary from 4×10^3 to 8×10^3 (0.02×10^2 to 3×10^2) cm^2 V^{-1} s^{-1}. The highest hole mobility of the order of 10^3 cm^2 V^{-1} s^{-1} has been obtained for ξ-As, η-As, and θ-As [Fig. 7]. The high hole mobility of these monolayers is mainly due to their very small deformation potentials (0.2–0.7 eV). The small deformation potentials of these monolayer allotropes correspond to the localized VBM charge carrier density [Fig. 6] that results in almost no change to the energy of these states by the displacement of phonons. Likewise, the highest electron mobility of the order of 10^3 cm^2 V^{-1} s^{-1} is calculated for β-As and O-As which is attributed to their relatively small electron effective masses (0.13 for β-As and 0.22 for O-As) [Table 3]. In order to find out the extent of anisotropy in carrier

Table 3 Calculated carrier effective masses (m^*) of electrons and holes at band edges. The m_e^* (m_h^*) represent electron (hole) effective masses, along the Γ–X and Γ–Y direction of the Brillouin zone. The deformation potential of electrons (E_d^e) and holes (E_d^h) along the *x* and *y* direction is given. The carrier effective masses and deformation potential for few monolayer allotropes have the same value along the *x* and *y* direction, so a single value for these monolayers is given

		m^* (m)		m_e^* (m)		m_h^* (m)		E_d^e (eV)		E_d^h (eV)	
Structure		CBM	VBM	*x*	*y*	*x*	*y*	*x*	*y*	*x*	*y*
(6-6)-As	A	0.78	0.16	1.29, 1.17[a]	0.39, 0.24[a]	1.57, 1.64[a]	0.21, 0.13[a]	3.5	1.4	2.1	7.2
	B	0.81	0.52	0.13, 0.128[b]		0.53, 0.501[b]		3.9		1.7	
	Γ	0.35	1.08	0.20	1.10	1.11	2.12	7.9	9.2	7.8	2.8
	Δ	0.67	0.54	0.96		0.69		3.2	4.8	2.3	3.8
	T	0.15	0.35	0.48	0.28	0.81	13.38	4.9	3.2	3.9	3.1
(4-8)-As	O	0.13	0.62	0.22		4.70		2.2		0.2	
	E	0.67	0.80	0.91		1.18		1.7		2.9	
	Ξ	0.45	1.09	0.55	4.85	1.73	1.52	1.9	6.2	0.2	0.2
(4-6-10)-As		0.52	1.88	5.51	0.32	3.28	4.02	2.9	0.8	0.7	0.6
Porous-As	H	0.76	0.75	1.40	3.47	3.52	1.68	4.6	4.7	0.3	0.4
	Θ	0.19	0.48	0.74	25.98	25.81	0.68	5.7	5.6	0.2	0.3
	HS	21.3	0.49	0.88		5.33		0.7		0.2	
	K	0.11	0.69	0.89	0.89	0.68	0.68	2.1	1.1	1.9	0.9

[a] Ref. 30. [b] Ref. 27.

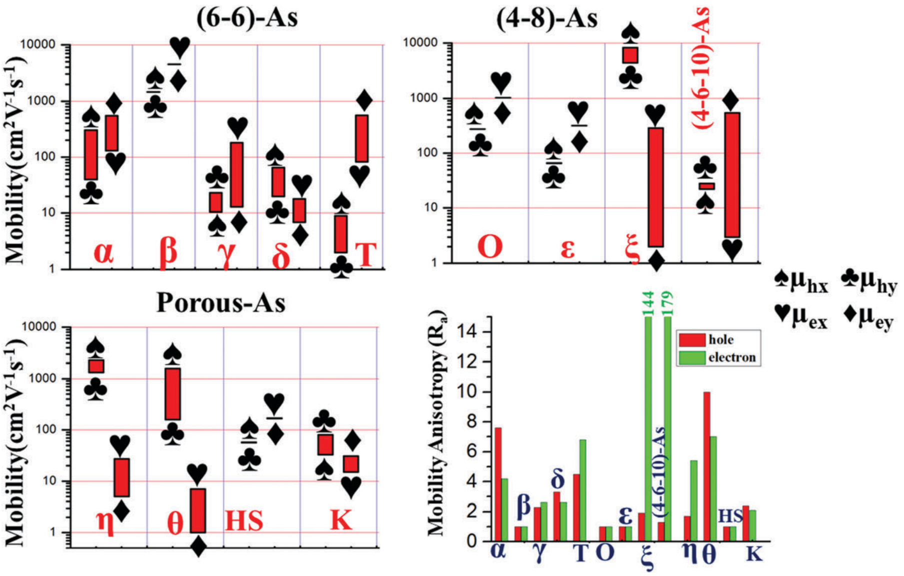

Fig. 7 The room temperature carrier mobilities of monolayer allotropes of As. μ_{hx} and μ_{hy} represent hole mobility along the *x* and *y* direction while μ_{ex} and μ_{ey} represent electron mobility along the *x* and *y* direction. Each bar for electron or hole mobility represents the upper and lower limit of the mobility of electrons or holes in a particular structure. The mobility anisotropy (R_a) is calculated as: R_a = Max(μ_x,μ_y)/Min(μ_x,μ_y).

mobilities, we now calculate the mobility anisotropy which is defined as:

$$R_a = \frac{\mathrm{Max}(\mu_x,\mu_y)}{\mathrm{Min}(\mu_x,\mu_y)} \tag{4}$$

R_a is equal to 1.0 for isotropic systems and is larger than 1.0 for anisotropic systems. The mobility anisotropy for both holes and electrons is given in Fig. 7. R_a is calculated to be 1.0 for β-As, O-As, ε-As and HS-As indicating isotropic carrier transport in these monolayers. Among the monolayer allotropes considered, the mobility anisotropy of electrons in ξ-As (144) and (4-6-10)-As (179) is calculated to be of the highest values. The mobility anisotropy of carriers for all other monolayer allotropes has been found to be between $1 < R_a < 10$.

It is worth comparing the calculated carrier mobilities of arsenene monolayers with important 2D materials such as graphene, black phosphorene and MoS_2. Graphene possesses the highest carrier mobility of the order of 10^4 cm^2 V^{-1} s^{-1}, whereas black phosphorene and monolayer MoS_2 exhibit a carrier mobility of the order of 10^3 cm^2 V^{-1} s^{-1} and 10^2 cm^2 V^{-1} s^{-1}, respectively.[51] We found that the electron and hole mobility of β-As; the hole mobility of ξ-As, η-As and θ-As; and the electron mobility of O-As, are comparable with black phosphorene, whereas, the electron and hole mobility of α-As; and the electron mobility of γ-As, T-As, ε-As, (4-6-10)-As and HS-As are comparable with monolayer MoS_2. Note that high intrinsic carrier mobilities play a crucial role in the performance of nanoelectronic devices based on layered structures.[1,2]

3.5 Potential application in photocatalytic water splitting

We now investigate the feasibility of the monolayer allotropes of arsenic to be used for photocatalytic water splitting. In general, a band gap of more than 1.23 eV is required for the photocatalysis reaction. At ambient conditions, the CBM must locate itself more negative than the redox potential of H^+/H_2, 0 V *vs.* normal hydrogen electrode (NHE) and the VBM must align more positive than the redox potential O_2/H_2O (1.23 V *vs.* NHE).[52] Band alignments of monolayer allotropes of arsenic with respect to the vacuum level in a neutral medium (pH = 7) are presented in Fig. 8. It is found that the band alignments and band gaps of β-As, γ-As, O-As, (4-6-10)-As, η-As, θ-As and HS-As allotropes match well with the redox potential of water, therefore, these monolayers can potentially be used for photocatalytic water splitting. Furthermore, their band gaps, except γ-As, lie in the visible region, so these 2D materials have promise and novelty to harvest visible light for photocatalytic splitting of water. It has been shown previously that strain engineering can tune the band gaps and band alignments of monolayers,[53] which further enhances the scope and usage of the studied

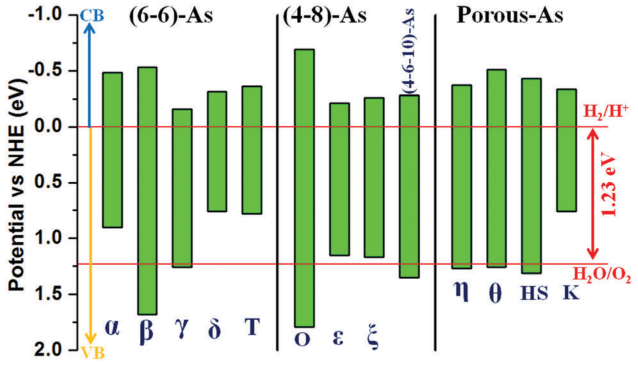

Fig. 8 Band energy alignment of the valance band maximum (VBM) and conduction band minimum (CBM) for monolayer allotropes of As at ambient conditions. The band edges relative to vacuum are calculated using the HSE06 functional. Horizontal red lines represent the water redox potential.

monolayer allotropes of arsenic for visible light driven photocatalytic water splitting. Despite the known toxicity of arsenene, it has emerged as a promising material for next-generation electronic and optoelectronic applications.[54,55] Recent fabrication of 2D arsenene nanosheets[56] is likely to pave the way for the use of arsenene in water splitting photocatalysis as suggested by this work.

4. Conclusions

We systematically investigated a wide variety of monolayer allotropes of arsenic using density functional theory. Through energetics and dynamical stability analysis we predict that besides honeycomb structures, the non-honeycomb and porous structures of monolayer arsenic are also stable. Results of cohesive energy and relative formation energy calculations show that these monolayer allotropes have the possibility of experimental fabrication. These monolayer structures are also found to be mechanically flexible and structural anisotropy gives rise to anisotropic elastic properties. We find that the considered monolayer allotropes cover a wide range of band gaps, which can be helpful for broad band photo-response. More importantly, these monolayers possess anisotropic carrier mobilities as high as several hundered square centimeters per volt-second. The high intrinsic mobilities of these monolayer allotropes may play a crucial role in the performance of nanoelectronic and optoelectronic devices based on arsenene. Considering the wide range of band gaps and high carrier mobility, these monolayers are found to be potential candidates for visible light driven photocatalytic water splitting.

Conflicts of interest

There are no conflicts to declare.

Acknowledgements

PJ is grateful to UGC New Delhi for providing financial assistance in the form of a UGC-BSR senior research fellowship. Usage of CV Raman HPC cluster (DST, New Delhi, Govt. of India funded) at Himachal Pradesh University, Shimla and Superior High Performance Computing cluster at Michigan Technological University Houghton, USA is gratefully acknowledged for obtaining results presented in this paper.

References

1 H. Liu, A. T. Neal, Z. Zhu, Z. Luo, X. Xu, D. Tomanek and P. D. Ye, Phosphorene: An Unexplored 2D Semiconductor with a High Hole Mobility, *ACS Nano*, 2014, **8**, 4033–4041.

2 L. Li, Y. Yu, G. J. Ye, Q. Ge, X. Ou, H. Wu, D. Feng, X. H. Chen and Y. Zhang, Black phosphorus field-effect transistors, *Nat. Nanotechnol.*, 2014, **9**, 372–377.

3 J. Qiao, X. Kong, Z. X. Hu, F. Yang and W. Ji, High-mobility transport anisotropy and linear dichroism in few-layer black phosphorus, *Nat. Commun.*, 2014, **5**, 4475.

4 J. W. Jiang and H. S. Park, Negative poisson's ratio in single-layer black phosphorus, *Nat. Commun.*, 2014, **5**, 4727.

5 Q. Liu, X. Zhang, L. B. Abdalla, A. Fazzio and A. Zunger, Switching a normal insulator into a topological insulator via electric field with application to phosphorene, *Nano Lett.*, 2015, **15**, 1222–1228.

6 R. Fei, A. Faghaninia, R. Soklaski, J. A. Yan, C. Lo and L. Yang, Enhanced thermoelectric efficiency via orthogonal electrical and thermal conductances in phosphorene, *Nano Lett.*, 2014, **14**, 6393–6399.

7 S. Zhang, S. Guo, Z. Chen, Y. Wang, H. Gao, J. G. Herrero, P. Ares, F. Zamora, Z. Zhu and H. Zeng, Recent progress in 2D group-VA semiconductors: from theory to experiment, *Chem. Soc. Rev.*, 2018, **47**, 982–1021.

8 M. Pumer and Z. Sofer, 2D Monoelemental Arsenene, Antimonene, and Bismuthene: Beyond Black Phosphorus, *Adv. Mater.*, 2017, **29**, 1605299.

9 J. Guan, Z. Zhu and D. Tomanek, Phase coexistence and metal insulator transition in few-layer phosphorene: A computational study, *Phys. Rev. Lett.*, 2014, **113**, 046804.

10 H. Wang, L. Xingxing, L. Pai and J. Yang, δ-Phosphorene: a two dimensional material with high negative Poisson's ratio, *Nanoscale*, 2017, **9**, 850–855.

11 M. Wu, H. Fu, L. Zhou, K. Yao and X. C. Zeng, Nine new phosphorene polymorphs with non-honeycomb structures: A much extended family, *Nano Lett.*, 2015, **15**, 3557.

12 T. Zhao, C. Y. He, S. Y. Ma, K. W. Zhang, X. Y. Peng, G. F. Xie and J. X. Zhong, A new phase of phosphorus: the missed tricycle type red phosphorene, *J. Phys.: Condens. Matter*, 2015, **27**, 265301.

13 Y. Zhang, Z. Wu, P. Gao, D. Fang, E. Zhang and S. Zhang, Structural, elastic, electronic, and optical properties of the tricycle-like phosphorene, *Phys. Chem. Chem. Phys.*, 2017, **19**, 2245–2251.

14 H. Wang, X. Li, Z. Liua and J. Yanga, ψ-Phosphorene: a new allotrope of phosphorene, *Phys. Chem. Chem. Phys.*, 2017, **19**, 2402.

15 P. Li and W. Luo, A new structure of two-dimensional allotropes of group V elements, *Sci. Rep.*, 2016, **6**, 25423.

16 F. Ersan, E. Akturk and S. Ciraci, Stable single-layer structure of group-V elements, *Phys. Rev. B*, 2016, **94**, 245417.

17 M. Xu, C. He, C. Zhang, C. Tang and J. Zhong, First-principles prediction of a novel hexagonal phosphorene allotrope, *Phys. Status Solidi RRL*, 2016, **10**, 563.

18 Z. Zhuo, X. Wu and J. Yang, Two-Dimensional Phosphorus Porous Polymorphs with Tunable Band Gaps, *J. Am. Chem. Soc.*, 2016, **138**, 7091–7098.

19 C. He, C. X. Zhang, C. Tang, T. Ouyang, J. Li and J. Zhong, Five low energy phosphorene allotropes constructed through gene segments recombination, *Sci. Rep.*, 2017, **7**, 46431.

20 C. Kamal and M. Ezawa, Arsenene: Two-dimensional buckled and puckered honeycomb arsenic systems, *Phys. Rev. B*, 2015, **91**, 085423.

21 S. Zhang, Z. Yan, Y. Li, Z. Chen and H. Zeng, Atomically thin arsenene and antimonene: semimetal-semiconductor and indirect-direct band-gap transitions, *Angew. Chem., Int. Ed.*, 2015, **54**, 3112–3115.

22 S. Mardanya, V. K. Thakur, S. Bhowmick and A. Agarwal, Four allotropes of semiconducting layered arsenic that switch into a topological insulator via an electric field: Computational study, *Phys. Rev. B*, 2016, **94**, 035423.

23 S. Y. Ma, P. Zhou, L. Z. Sun and K. W. Zhang, Two-dimensional tricycle arsenene with a direct band gap, *Phys. Chem. Chem. Phys.*, 2017, **18**, 8723–8729.

24 S. Zhang, M. Xie, F. Li, Z. Yan, Y. Li, E. Kan, W. Liu, Z. Chen and H. Zeng, Semiconducting group 15 monolayers: a broad range of band gaps and high carrier mobilities, *Angew. Chem.*, 2015, **127**, 1–5.

25 Z. Zhang, J. Xie, D. Yang, Y. Wang, M. Si and D. Xue, Manifestation of unexpected semiconducting properties in few-layer orthorhombic arsenene, *Appl. Phys. Express*, 2015, **8**, 055201.

26 C. Wang, Q. Xia, Y. Nie, M. Rahman and G. Guo, Strain engineering band gap, effective mass and anisotropic Dirac-like cone in monolayer arsenene, *AIP Adv.*, 2016, **6**, 035204.

27 G. Pizzi, M. Gibertini, E. Dib, N. Marzari, G. Iannaccone and G. Fiori, Performance of arsenene and antimonene double-gate MOSFETs from first principles, *Nat. Commun.*, 2016, **7**, 12585.

28 S. Sharma, S. Kumar and U. Schwingenschlogl, Arsenene and Antimonene: Two-dimensional materials with high thermoelectric figures of Merit, *Phys. Rev. Appl.*, 2017, **8**, 044013.

29 Y. Wang, P. Huang, M. Ye, R. Quhe, Y. Pan, H. Zhang, H. Zhong, J. Shi and J. Lu, Many-body effect, carrier mobility, and device performance of hexagonal Arsenene and Antimonene, *Chem. Mater.*, 2017, **29**, 2191–2201.

30 B. Peng, H. Zhang, H. Shao, K. Xu, G. Ni, J. Li, H. Zhua and C. M. Soukoulis, Chemical intuition for high thermoelectric performance in monolayer black phosphorus, a-arsenene and aW-antimonene, *J. Mater. Chem. A*, 2018, **6**, 2018–2033.

31 D. Kecik, E. Durgun and S. Ciraci, Optical properties of single-layer and bilayer arsenene phases, *Phys. Rev. B*, 2016, **94**, 035423.

32 S. Nahas, A. Bajaj and S. Bhowmick, Polymorphs of two dimensional phosphorus and arsenic: An insight from evolutionary search, *Phys. Chem. Chem. Phys.*, 2017, **11**, 11282–11288.

33 J. Carrete, L. J. Gallego and N. Mingo, Structural complexity and phonon physics in 2D arsenenes, *J. Phys. Chem. Lett.*, 2017, **8**, 1375–1380.

34 P. Jamdagni, A. Kumar, A. Thakur, R. Pandey and P. K. Ahluwalia, Tunneling characterstics of Stone-Wales defects in monolayers of Sn and group-V elements, *J. Phys.: Condens. Matter*, 2017, **29**, 395501.

35 J. L. Zhang, S. Zhao, C. Han, Z. Wang, S. Zhong, S. Sun, R. Guo, X. Zhou, C. Gu, K. Yuan, Z. Li and W. Chen, Epitaxial growth of single layer blue phosphorus: A new phase of two-dimensional phosphorus, *Nano Lett.*, 2016, **16**, 4903–4908.

36 J. Guan, Z. Zhu and D. Tomanek, Semiconducting layered blue phosphorus: A computational study, *Phys. Rev. Lett.*, 2014, **112**, 176802.

37 G. Kresse and J. Furthmuller, Efficient iterative schemes for *ab initio* total-energy calculations using a plane-wave basis set, *Phys. Rev. B*, 1996, **54**, 11169.

38 J. P. Perdew, K. Burke and M. Ernzerhof, Generalized Gradient Approximation Made Simple, *Phys. Rev. Lett.*, 1996, **77**, 3865.

39 P. E. Blochl, Projector augmented-wave method, *Phys. Rev. B*, 1994, **50**, 17953.

40 S. Grimme, Semiempirical GGA-type density functional constructed with a long-range dispersion correction, *J. Comput. Chem.*, 2006, **27**, 1787.

41 J. Heyd, G. E. Scuseria and M. Ernzerh, Hybrid functionals based on screened Coulomb potential, *J. Chem. Phys.*, 2006, **118**, 8207.

42 J. Paier, M. Marsman, K. Hummer, G. Kresse, I. C. Gerber and J. G. Angyan, Screened hybrid density functionals applied to solids, *J. Chem. Phys.*, 2006, **125**, 249901.

43 J. Bardeen and W. Shockley, Deformation potentials and mobilities in non-polar crystals, *Phys. Rev.*, 1950, **80**, 72–80.

44 H. Wang, Y. Pei, A. D. LaLonde and G. J. Snyder, Weak electron-phonon coupling contributing to high thermoelectric performance in n-type PbSe, *PANS*, 2012, **109**, 9705.

45 D. Schifer and C. S. Barrett, The crystal structure of arsenic at 4.2, 78 and 2990 K, *J. Appl. Crystallogr.*, 1969, **2**, 30.

46 H. Sahin, S. Cahangirov, M. Topsakal, E. Bekaroglu, E. Akturk, R. T. Senger and S. Ciraci, Monolayer honeycomb structures of group-IV elements and III–V binary compounds: First-principles calculations, *Phys. Rev. B*, 2009, **80**, 155453.

47 A. Falin, Q. Cai, E. J. G. Santos, D. Scullion, D. Qian, R. Zhang, Z. Yang, S. Huang, K. Watanabe, T. Taniguchi, M. R. Barnett, Y. Chen, R. S. Ruoff and L. H. Li, Mechanical properties of atomically thin boron nitride and the role of interlayer interactions, *ACS Nano*, 2017, **8**, 15815.

48 S. Bertolazzi, J. Brivio and A. Kis, Stretching and Breaking of Ultrathin MoS_2, *ACS Nano*, 2011, **12**, 9703.

49 A. Kumar and P. K. Ahluwalia, Electronic Structure of Transition Metal Dichalcogenides Monolayer 1H-MX_2 (M = Mo, W; X = S, Se, Te) from *ab initio* Theory: New Direct Band Gap Semiconductors, *Eur. Phys. J. B*, 2012, **85**, 186.

50 P. Jamdagni, A. Kumar, A. Thakur, R. Pandey and P. K. Ahluwalia, Stability and electronic properties of SiGe-based 2D layered structures, *Mater. Res. Express*, 2015, **2**, 016301.

51 N. Petrone and J. Hone, Two-dimensional flexible nanoelectronics, *Nat. Commun.*, 2014, **5**, 5678.

52 V. Chakrapani, J. C. Angus, A. B. Anderson, S. D. Wolter, B. R. Stoner and G. U. Sumanasekera, Charge transfer equilibria between diamond and an aqueous oxygen electrochemical redox couple, *Science*, 2007, **318**, 1424.

53 B. Sa, Y. L. Li, J. Qi, R. Ahuja and Z. Sun, Strain engineering for phosphorene: The potential application as a photocatalys, *J. Phys. Chem. C*, 2014, **118**, 26560–26568.

54 Y. Wang, M. Ye, M. Weng, J. Li, X. Zhang, H. Zhang, Y. Guo, Y. Pan, L. Xiao, J. Liu, F. Pan and J. Lu, Electrical contacts in monolayer arsenene devices, *ACS Appl. Mater. Interface*, 2017, **9**, 29273–29284.

55 M. Hart, J. Chen, A. Michaelides, A. Sella, M. S. P. Shaffer and C. G. Salzmann, One-dimensional arsenic allotropes: polymerization of yellow arsenic inside single-wall carbon nanotubes, *Angew. Chem., Int. Ed.*, 2018, **57**, 1–6.

56 P. Vishnoi, M. Mazumder, S. K. Pati and C. N. R. Rao, Arsenene nanosheets and nanodots, *New J. Chem.*, 2018, **42**, 14091–14095.